Simulations of beam-matter interaction experiments at the CERN HiRadMat facility and prospects of high-energy-density physics research

N. A. Tahir,[1] F. Burkart,[2] A. Shutov,[3] R. Schmidt,[4] D. Wollmann,[4] and A. R. Piriz[5]

[1]*GSI Helmholtzzentrum für Schwerionenforschung, Planckstraße 1, DE-64291 Darmstadt, Germany*

[2]*CERN-AB, CH-1211 Geneva 23, Switzerland and University of Frankfurt, DE-60323 Frankfort, Germany*

[3]*Institute of Problems of Chemical Physics, Russian Academy of Sciences, 142432 Chernogolovka, Russia*

[4]*CERN-AB, CH-1211 Geneva 23, Switzerland*

[5]*E.T.S.I. Industriales, Universidad de Castilla-La Mancha, ES-13071 Ciudad Real, Spain*

(Received 20 August 2014; published 18 December 2014)

In a recent publication [Schmidt *et al.*, Phys. Plasmas **21**, 080701 (2014)], we reported results on beam-target interaction experiments that have been carried out at the CERN HiRadMat (High Radiation to Materials) facility using extended solid copper cylindrical targets that were irradiated with a 440-GeV proton beam delivered by the Super Proton Synchrotron (SPS). On the one hand, these experiments confirmed the existence of hydrodynamic tunneling of the protons that leads to substantial increase in the range of the protons and the corresponding hadron shower in the target, a phenomenon predicted by our previous theoretical investigations [Tahir *et al.*, Phys. Rev. ST Accel. Beams **25**, 051003 (2012)]. On the other hand, these experiments demonstrated that the beam heated part of the target is severely damaged and is converted into different phases of high energy density (HED) matter, as suggested by our previous theoretical studies [Phys. Rev. E **79**, 046410 (2009)]. The latter confirms that the HiRadMat facility can be used to study HED physics. In the present paper, we give details of the numerical simulations carried out to understand the experimental measurements. These include the evolution of the physical parameters, for example, density, temperature, pressure, and the internal energy in the target, during and after the irradiation. This information is important in order to determine the region of the HED phase diagram that can be accessed in such experiments. These simulations have been done using the energy deposition code FLUKA and a two–dimensional hydrodynamic code, BIG2, iteratively.

DOI: 10.1103/PhysRevE.90.063112 PACS number(s): 51.50.+v, 29.27.−a, 51.60.+a

I. INTRODUCTION

Bunched and well-focused intense particle beams have emerged as a very efficient, novel tool to research numerous areas of physics in previously unaccessed parameter range. The new generation of powerful accelerators, like the Large Hadron Collider (LHC) at CERN [1], has already been operational for some time, while others including Facility for Antiprotons and Ion Research (FAIR) [2–4] at Darmstadt, Germany and On-line Production System of Radioactive Ions 2nd generation (SPIRAL2) [5] at Caen, France, are under construction. Moreover, the possibility of building a much more powerful accelerator named the Future Circular Collider (FCC) with a tunnel extending up to an 80-km circumference, is currently being discussed at CERN. In view of these developments and others across the world, the recent beam-target experiments performed at the HiRadMat facility, are of considerable importance as these results have serious implications for the machine protection system design for powerful accelerators [6]. In addition to that, these experiments have clearly demonstrated that intense particle beams are a very effective tool to generate high energy density (HED) matter in the laboratory. This suggests that all accelerator facilities in the world that are capable of delivering well-focused, bunched intense particle beams, are very much suited for HED physics research, which could be an important additional application of such machines. In the present paper we emphasize this latter aspect of the HIRadMat experiments.

It is to be noted that HED physics includes numerous areas of basic and applied physics, for example, plasma physics, condensed matter physics, high pressure physics, astrophysics, planetary physics, inertial confinement fusion, and many others. Over the past decades, static as well as dynamic techniques have been used to generate samples of HED matter in the laboratory. The most popular tool used in the former scheme is a diamond anvil cell [7,8] while in the latter configuration, shock compression is used for this purpose. Traditional shock wave generators mainly include high power explosives [9], gas guns [10], Z pinches [11], and high power lasers. [12,13]. In a few special experiments, even nuclear explosions have been used for this purpose [14]. Intense particle beams offer much more flexibility compared to other drivers because they can generate HED matter using two completely different dynamic schemes. One scheme relies on isochoric and uniform heating of matter by the projectile ions that directly induces HED states in the target [15–17], whereas the second scheme involves shock compression of matter [18–27]. Moreover, due to the large efficiency and high repetition rate of an ion accelerator, intense ion beams are believed to be a viable driver for inertial fusion [28–35].

It is also to be noted that unlike in the HED physics and inertial confinement fusion problems, in some other type of experiments, the target must not be damaged but should maintain its original state during the entire experimental campaign, which of course, is very difficult to achieve due to the high level of specific power deposition by the beam. For example, the production target in the Super-FRS experiments to be carried out at FAIR to generate radioactive ion beams [36–40]. In addition, the design of thin foils for charge stripping of high current ion beams, faces similar problems [41–43]. In general, the impact of a focused intense ion beam

on a target, induces HED states in the material. In Sec. II we discuss some special features of the beam-target interaction problem while in Sec. III we describe the High Radiation to Materials (HiRadMat) facility and important characteristics of the Super Proton Synchrotron (SPS). Section IV shows the beam and the target parameters considered in this work, whereas the numerical simulation results are presented in Sec. V. Conclusions drawn from this work are noted in Sec. VI.

II. PROBLEM DEFINITION

The LHC is the most powerful and most complex accelerator that has ever been built by human kind. Working at its full capacity, it is expected to accelerate two counter-rotating beams of 7-TeV protons, each carrying an energy of 360 MJ, capable of melting 500 kg of copper. Ensuring safe operation of the machine with such powerful beams is an extremely important and challenging problem. Any uncontrolled release of the beam energy could cause serious damage to the equipment. A rapid loss of even 0.002% of the 7-TeV/c beam at one spot could already damage a high-Z material like copper. A worst-case scenario is the possibility of the full LHC beam being lost at one place. Although the probability of an accident of this magnitude is extremely small, nevertheless it is important to have full knowledge of the consequences if it ever happens. This information is essential in order to design the protection systems of the machine correctly, to set admissible risk levels, and to determine the inventory of the spare parts needed to possibly replace the damaged equipment.

Extensive theoretical work has been carried out over the past 10 years to study the effect of the full impact of an LHC beam on cylindrical solid copper and carbon targets [16,44–46]. According to the nominal design parameters, each beam comprises a bunch train with every bunch consisting of 1.15×10^{11} protons. The total number of bunches per beam is 2808 so that the total number of protons per beam is about 3×10^{14}. The bunch length is 0.5 ns and two neighboring bunches are separated by 25 ns while intensity distribution in the radial direction is Gaussian with a standard deviation, $\sigma = 0.2$ mm. The total duration of the beam is of the order of 89 μs. The theoretical investigations of the beam-target heating problem showed that the energy deposited by a few tens of proton bunches leads to strong heating that produces very high pressure in the beam heated region. This high pressure generates radially outgoing shock waves that leads to a continuous density reduction at the target center. As a consequence, the protons that are delivered in the subsequent bunches, and the hadronic shower they generate, penetrate deeper into the target. Continuation of this process leads to a substantial increase in the range of the projectile particles and their hadronic shower. For example, in case of a solid copper target, the static range of the 7-TeV protons and their shower is about 1 m. However, when a full hydrodynamic calculation is done using the entire beam (duration 89 μs), the penetration depth becomes about 35 m. This phenomenon is named "hydrodynamic tunneling" of the protons and has very important implications for the machine protection design of every powerful accelerator. Due to these reasons, dedicated experiments were performed at the HiRadMat facility to investigate this effect using the 440-GeV SPS proton beam. These experiments not only confirmed the existence of the hydrodynamic tunneling phenomenon, but they also demonstrated that this facility can equally be useful to study HED-physics-related problems.

III. THE HIGH RADIATION TO MATERIALS FACILITY AT CERN AND THE SUPER PROTON SYNCHROTRON

The High Radiation to Materials (HiRadMat) facility at CERN is used to irradiate materials and accelerator components (mainly for the LHC) with high intensity, high density, and pulsed proton or ion beams, to study the effects due to beam impacts. This beam is extracted from the SPS, which not only is used as the LHC injector, but also to accelerate and extract protons and ions (such as lead and other ion species) for fixed target experiments, like the ones reported in [47,48].

The SPS accelerator is 6.9-km long (circumference) and accelerates protons from 14 GeV/c or 26 GeV/c to a momentum of up to 440 GeV/c. It is a cycling machine with cycles having a length of about 15 s. The transverse beam size is largest at injection and decreases with the square root of the beam energy during acceleration. For the operation as a synchrotron, the beam size is typically of the order of 1 mm.

When the SPS operates as the LHC injector, up to 288 bunches are accelerated, each bunch with about 1.15×10^{11} protons (nominal parameters). The bunch length is 0.5 ns and two neighboring bunches are separated by 25 ns so that the duration of the entire beam is 7.2 μs. The normalized emittance is 3.75×10^{-6}m. Assuming a beta function of 100 m, the beam size is characterized with σ of about 0.88 mm. When the SPS was used as a proton-antiproton collider, the luminosity was maximized by minimizing the beta function to 0.5 m. Assuming this value, the beam size would be as small as with $\sigma = 0.06$ mm.

A summary of the beam properties is shown in Table I. It is seen that the maximum bunch intensity can be up to 1.7×10^{11} particles and the focal size can go down to 0.1 mm $\sigma_{\rm rms}$, thus providing a very dense beam (energy per size). The spot size can be tuned from $\sigma = 0.1$ to 2 mm. The experimental area has a length of more than 9 m that allows up to three experiments to be installed in parallel.

TABLE I. HiRadMat beam properties.

Parameter	Symbol	Protons	Pb ions
Particle energy	E	440 GeV	36.9 TeV
Bunch intensity	N_b	1.7×10^{11}	7×10^7
Max. number of bunches per pulse	$n_{\rm max}$	288	52
Max. pulse intensity	$N_p = n_{\rm max} N_b$	4.9×10^{13} protons	3.64×10^9 ions
Bunch spacing	Δt_b	25 ns	100 ns
Min. beam size (rms)	$\sigma_{\rm beam}$	0.1 mm	0.1 mm
RMS bunch length	σ_z	11.24 cm	11.24 cm
Pulse length	t_p	7.2 μs	5.2 μs

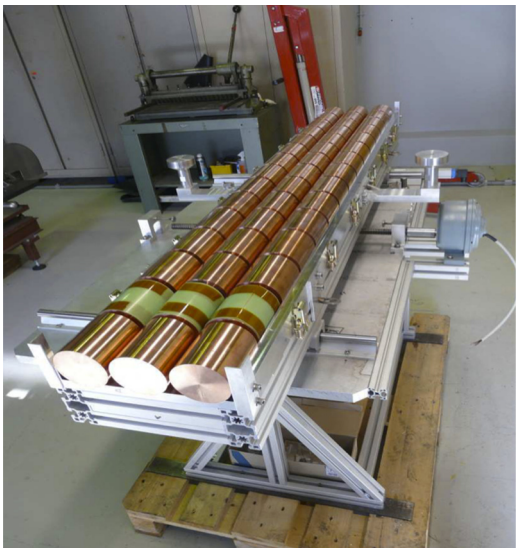

FIG. 1. (Color online) Three target assemblies used in the experiments, each comprising 15 solid Cu cylinders; every cylinder has radius, $r = 4$ cm, length, $L = 10$ cm, and 1 cm separation in between.

IV. BEAM AND TARGET PARAMETERS

The target assembly used in the experiments before it is installed in the HiRadMat facility is shown in Fig. 1. It consists of three targets, each comprising 15 copper cylinders with a spacing of 1 cm in between that allows for visual inspection of the targets after irradiation. Each cylinder has a radius, $r = 4$ cm and length, $L = 10$ cm. The three target cylinders are enclosed in an aluminum housing with a top cover that provides stability to the setup and prevents contamination of the facility as well. The target assembly is mounted onto a movable table which can be moved to four different positions, namely to Target 1, Target 2, Target 3, and the off-beam position, thereby leading to transverse irradiation of the left face of the first cylinder of the different targets used in the experiment.

In these experiments the proton energy was 440 GeV, bunch intensity was 1.5×10^{11} protons, bunch length was 0.5 ns, and bunch separation was 50 ns. Target 1 was irradiated with 144 bunches with a beam focal spot characterized by $\sigma = 2$ mm (Experiment 1). Target 2 was irradiated with 108 bunches, whereas Target 3 was irradiated with 144 bunches while in both these cases, the beam had a much smaller focal spot size characterized by $\sigma = 0.2$ mm. The latter two experiments were named Experiment 2 and Experiment 3, respectively. A summary of the beam parameters used in these three experiments is presented in Table II.

TABLE II. Experimental beam parameters used in the three experiments.

Target	Number of bunches	Beam σ (mm)	Beam energy (MJ)
1	144	2.00	1.52
2	108	0.20	1.14
3	144	0.20	1.52

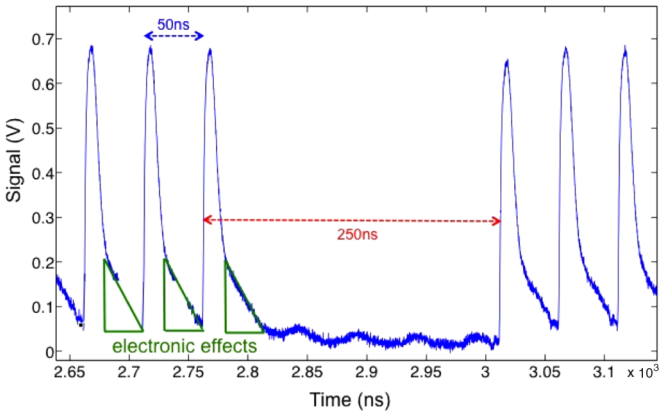

FIG. 2. (Color online) Time structure of the proton beam.

The temporal profile of the beam is presented in Fig. 2. In fact the protons were delivered in sets of 36 bunches each, while a separation of 250 ns was considered between the neighboring bunch packets.

In the simulations we use exactly the same beam parameters as in the experiments, but a slightly modified target design is used to simplify the calculations. Instead of considering 15 cylinders in a target, we use a single copper cylinder that has a total length of 150 cm (equivalent length of copper) and a radius of 4 cm. This is a good approximation as the hydrodynamic effects in this type of problems are much stronger in the radial direction than in the axial direction. Excellent agreement between the experimental measurements and the simulations reported in [47], underscores the validity of this approximation.

V. NUMERICAL SIMULATION RESULTS

In this section we present the numerical simulations of the thermodynamic and hydrodynamic behavior of a solid copper cylinder which has a length of 150 cm and a radius of 4 cm, that is impacted by 440-GeV proton bunches delivered by the SPS beam. The beam is incident perpendicular to the left face of the target. These calculations have been done in two steps.

First, the energy deposition in the target from protons is calculated using the FLUKA code [49,50], assuming solid copper density. FLUKA is an established particle interaction and Monte Carlo package capable of simulating all components of the particle cascades in matter, up to multi-TeV energies. Second, this energy deposition data are used as input to a sophisticated two–dimensional hydrodynamic code, BIG2 [51], to calculate the beam-target interaction that causes hydrodynamic motion, mainly in the radial direction, which leads to density reduction at the target center. It is to be noted that the full three-dimensional energy deposition distribution calculated by FLUKA is azimuthally symmetric that allows for the use of two-dimensional hydrodynamic simulations of the beam-target heating. Multiphase, multicomponent equation of state (EOS) data from [52,53] are used in BIG2 to model different physical states of copper during and after the irradiation. The hydrocode is allowed to operate until the density reduction at the target center becomes of the order of 15%. The BIG2

code is then stopped and the modified density distribution obtained from the hydrodynamic calculations is used back in the FLUKA code to calculate the corresponding modified energy deposition distribution for the bunches arriving subsequently. This new distribution is then used in the BIG2 code as the next step. In this manner, the two codes are run iteratively. In the present simulations the iteration step comes out to be 700 ns. We also note that the simulations have been done only for Experiment 2 and Experiment 3, in which we used the smaller focal spot size characterized with σ = 0.2 mm. This is because the hydrodynamic tunneling was more visible in these two experiments compared to Experiment 1.

A. Proton energy deposition calculations using FLUKA

For the study presented in this paper, the geometry for the FLUKA calculations is considered to be a cylinder of solid copper with radius = 4 cm, length = 150 cm, and having a density of 8.93 g/cm^3. The energy deposition is obtained using a two-dimensional Gaussian beam distribution (horizontal and vertical = with $\sigma_{\rm rms} = 0.2$ mm) that was incident perpendicular to the front face of the cylinder. This beam size was selected for the simulations since it corresponds to the size of the beam used in the experiments.

In Fig. 3(a), we present the energy deposition distribution per 440 GeV proton in units GeV/g as calculated by FLUKA, assuming solid material density. These data show that the range of the shower is about 65 cm in the target and the peak value of the distribution is around 3.75 GeV/p/g. The FLUKA calculations also suggest that approximately 40% beam energy escapes while 60% is absorbed in the target. The total energy in a single proton bunch is 10.56 kJ which means every bunch deposited 6.25 kJ in the target.

Figure 3(b) presents the energy deposition data obtained with FLUKA, but using the density distribution provided by BIG2 at $t = 3.73\,\mu$s. The energy deposition distribution has been modified with a broadening of the energy peak that indicates deeper penetration of the protons and the shower into the target. The maximum value of the energy deposition has been reduced to around 2.4 GeV/p/g.

The energy deposition distribution plotted in Fig. 3(c) has been calculated by FLUKA, using the density distribution obtained from BIG2 at $t = 4.75\,\mu$s. This figure shows a significant broadening of the energy peak while the maximum value of the energy deposition becomes about 1.6 GeV/p/g. This indicates a much longer penetration of the particle shower in the target.

Figure 3(d) presents energy deposition distribution at $t = 6.75\,\mu$s. It is interesting to note that the distribution has a double peak behavior and the second peak is higher than the first one. This is due to the fact that the density in the initially irradiated region of the target has decreased to such an extent that it contributes very little to the beam stopping and the protons and the shower penetrate much deeper into the target, thereby generating the second peak in the energy distribution.

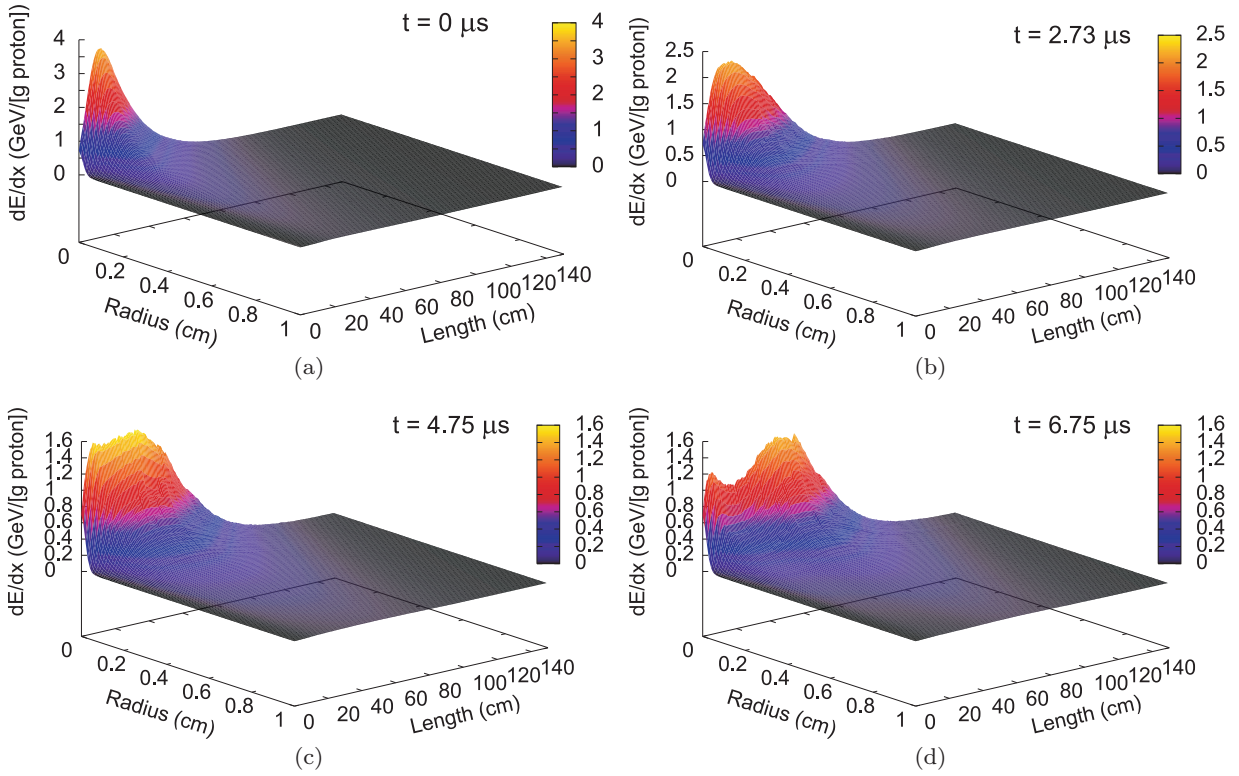

FIG. 3. (Color online) FLUKA calculations of energy deposition of a single 440-GeV SPS proton in a solid copper cylinder having radius, $r = 4$ cm, length, $L = 150$ cm, with facial irradiation, beam spot size characterized by standard deviation, $\sigma = 0.2$ mm; (a) using solid density of 8.93 g/cm^3; (b) using the density distribution provided by the BIG2 at $t = 2.73\mu$s; (c) using the density distribution provided by the BIG2 at $t = 4.75\,\mu$s; (d) using the density distribution provided by the BIG2 at $t = 6.75\,\mu$s.

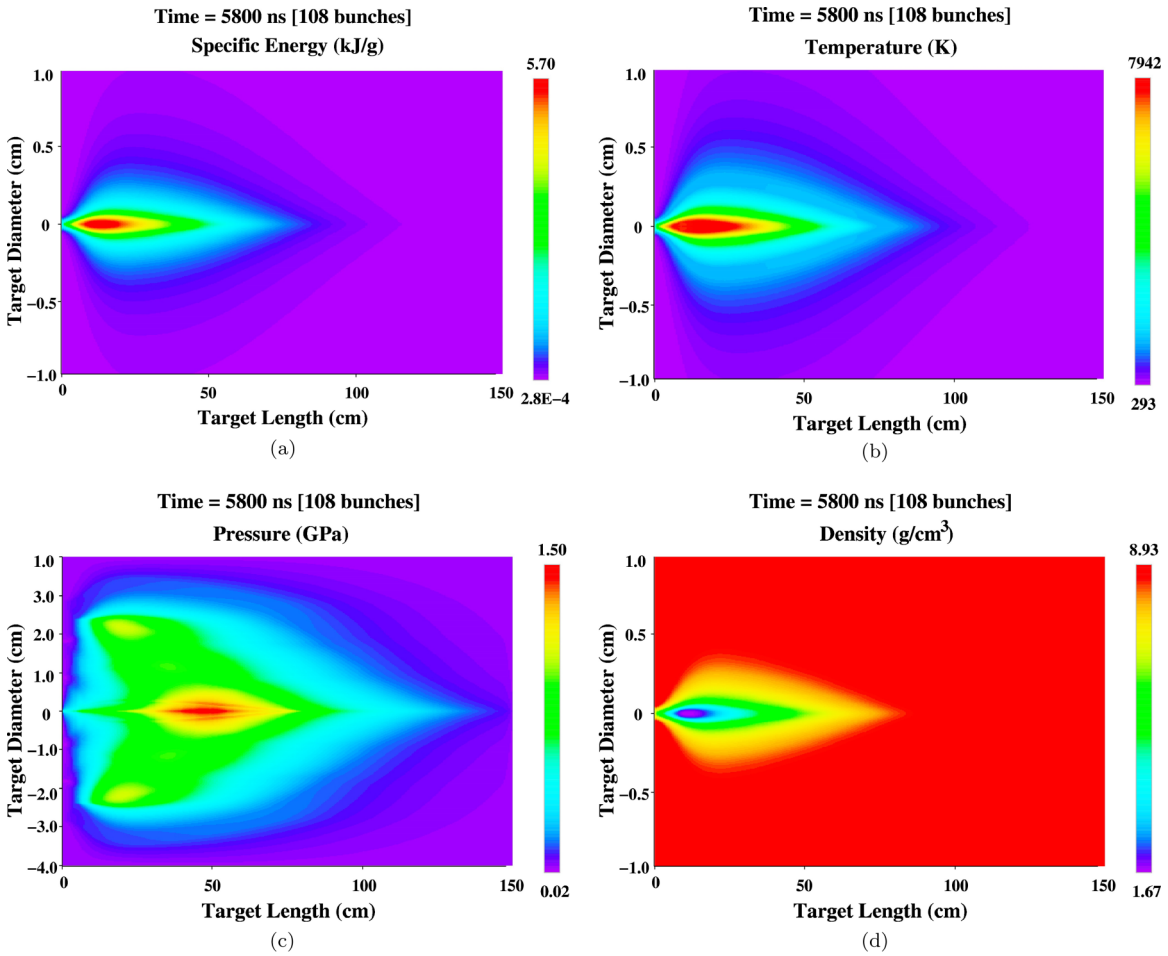

FIG. 4. (Color online) Target physical conditions calculated by BIG2 at $t = 5800$ ns time when 108 bunches of 440-GeV protons with focal spot $\sigma = 0.2$ mm, bunch intensity $= 1.5 \times 10^{11}$ protons, bunch length $= 0.5$ ns, and bunch separation $= 50$ ns, have been delivered (Experiment 2); (a) specific energy deposition distribution; (b) temperature distribution; (c) pressure distribution; (d) density distribution.

B. Hydrodynamic simulations using BIG2

For the BIG2 simulations, we consider the same target as the one used in the FLUKA calculations, namely, a solid copper cylinder, 150-cm long with a radius = 4 cm. In the first iteration, we use as input to the BIG2 code, the energy loss data calculated by FLUKA assuming a solid target density of 8.93 g/cm^3 that is presented in Fig. 3(a). The BIG2 code is allowed to run for one iteration step of 700 ns when the density at the target center is reduced by about 15%. This modified density distribution is then used in the FLUKA code to calculate the corresponding energy loss distribution which is again used in the BIG2 code for the second iteration. In this manner the two codes are applied iteratively to the problem of beam-matter heating.

In Fig. 4(a) we present the specific energy deposition in the target at $t = 5800$ ns, time when 108 bunches have been delivered that means the heating time of one of the experiments (Experiment 2). It is seen that by this time, a maximum specific energy of 5.7 kJ/g has been deposited at the target center which gives rise to strong heating that leads to a maximum temperature of about 7900 K in the beam heated zone [see Fig. 4(b)]. The corresponding pressure distribution is presented in Fig. 4(c) which shows a maximum pressure of 1.5 GPa and the high pressure region has spread in large part of the target due to the shock wave propagation in the radial direction. It is to be noted that the target heating is a localized effect and we therefore present the specific energy and the temperature distributions, only for the inner 1-cm cylinder radius. The hydrodynamics, on the other hand, is a global phenomenon as the pressure waves travel throughout the target. It is therefore necessary to show the pressure distribution in the entire target.

The corresponding density distribution is presented in Fig. 4(d) which shows that the density at the target center has been reduced to 1.67 g/cm^3 which is about 19% of the solid copper density. It is also to be noted that the direct heating of the material has extended to about 80 cm in the longitudinal direction due to the hydrodynamic tunneling effect, which is in full agreement with the experimental measurements [47]. The pressure wave, on the other hand, has traveled along almost the entire cylinder length.

In Figs. 5(a)–5(d) are plotted the same variables as in Figs. 4(a)–4(d), respectively, but at $t = 7850$ ns, when 144 proton bunches have been delivered which represents Experiment 3. Figure 5(a) shows that a maximum specific energy of 6.3 kJ/g has been deposited at the target center that leads to a temperature of about 7600 K [see Fig. 5(b)]. It is interesting to note that the maximum temperature in this case is somewhat lower than that in Fig. 4(b), which is due to

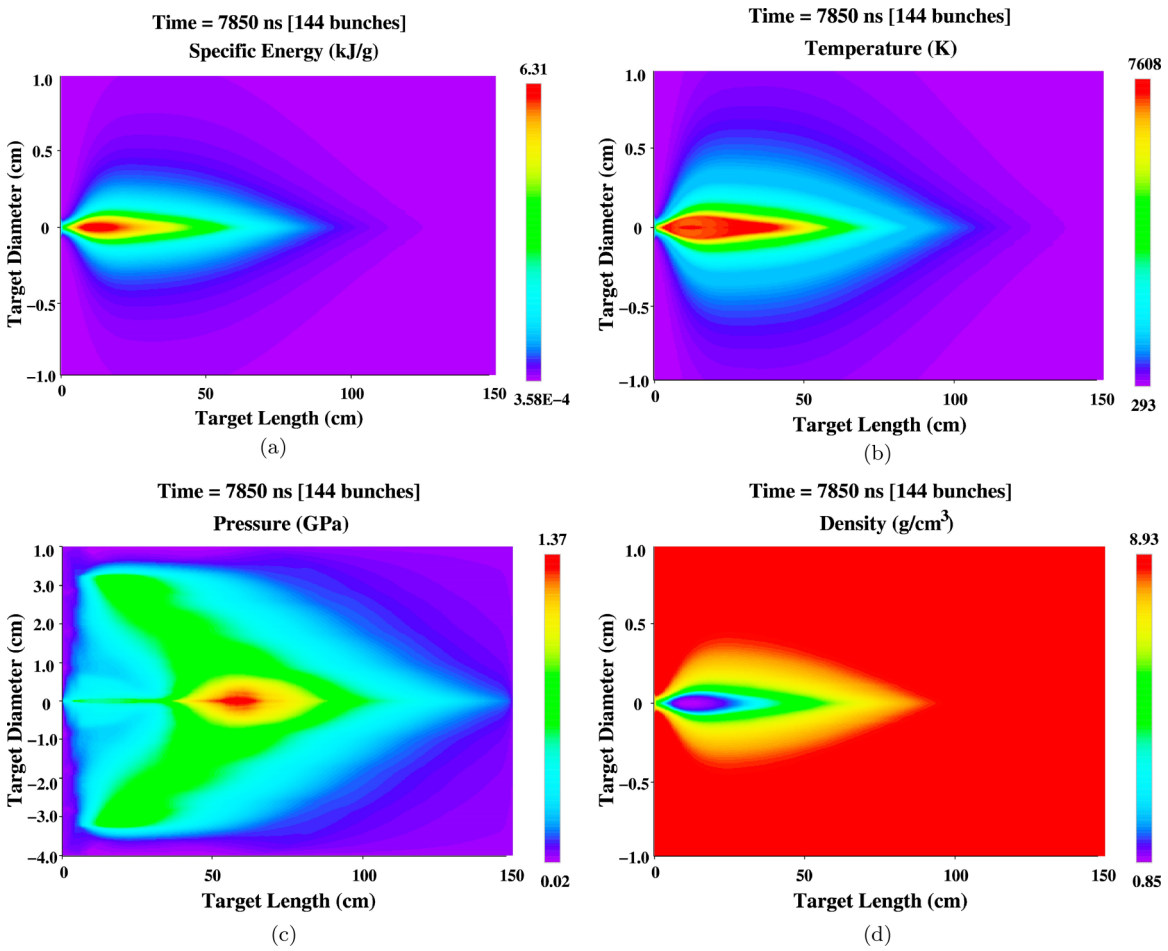

FIG. 5. (Color online) Same as in Fig. 4, but at $t = 7850$ ns, when 144 bunches have been delivered (Experiment 3).

the cooling caused by material expansion resulting from the hydrodynamic effects.

It is seen in Fig. 5(c) that the pressure waves have traveled throughout the target in the radial as well as in the longitudinal direction. The radial waves have already been reflected at the target surface whereas the high pressure region has also been extended to the opposite face of the target.

The corresponding density distribution is presented in Fig. 5(d) which shows that by this time, the density at the target center has been depleted to 0.85 g/cm^3 which is about 10% of the solid copper density.

In order to have a quantitative understanding of the simulation results, we plot in Fig. 6(a), the temperature profiles along the target axis ($r = 0.0$) at four different times when 36, 72, 108, and 144 proton bunches, respectively, have been delivered. The flat region on the right part of each curve represents the melting of the material. It is clearly seen that the melting zone propagates towards the right direction due to the deeper penetration of the protons resulting from the hydrodynamic tunneling. The reduction in the temperature in the low density region above the point $L = 25$ cm is shown in the curve corresponding to 144 bunches.

Figure 6(b) shows the same four profiles as Fig. 5(a) along the target length, but at $r = 1$ mm. It is seen that the specific energy is still high enough to melt the material at this distance from the axis and a maximum temperature of 5000 K is achieved around the region at $L = 25$ cm after 144 proton bunches have been delivered.

Figure 6(c) shows the same temperature profiles as the previous two figures, but at $r = 2$ mm. It is seen that even at this distance from the axis, the material is melted and is heated to a maximum temperature of 2500 K after the delivery of 144 proton bunches.

In Fig. 7(a) we plot the density profiles corresponding to the temperature profiles presented in Fig. 6(a). It is seen that the density is systematically being reduced as more bunches deposit their energy and the minimum density becomes less than 1 g/cm^3 after the delivery of 144 bunches. This shows serious damage to the target along the axis.

Figure 7(b) shows the same density profiles as Fig. 7(a), but at a radial position of 1 mm. Significant density reduction is also clearly visible in this region and the minimum density becomes about 5.5 g/cm^3 after 144 bunches are delivered. Figure 7(c) shows the density vs target length at a radial position of 2 mm for the four different cases considered in the previous two figures. Again, a noticeable density reduction can be observed in this region.

The above analysis of the simulation results shows that a significant part of the target undergoes phase transitions and enters into the regime of the HED state of copper. In Fig. 8 we plot the phase state of the target at $t = 7850$ ns which is the time when 144 proton bunches have been delivered

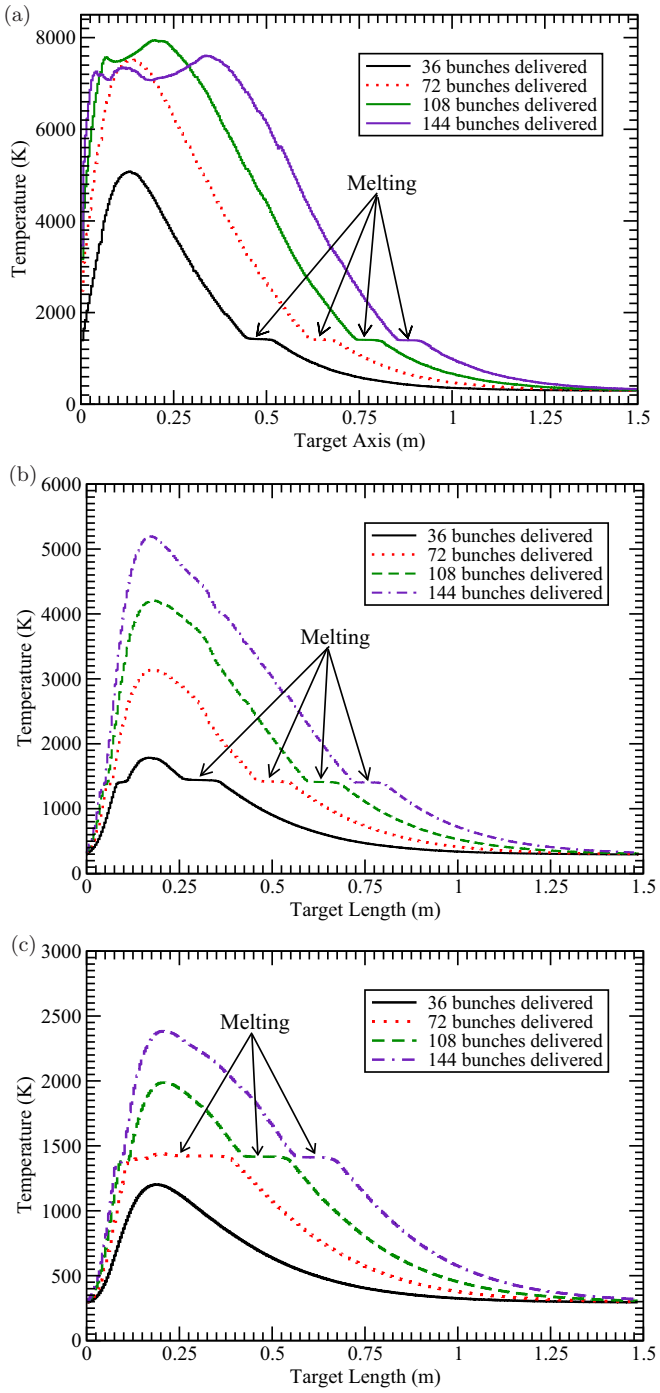

FIG. 6. (Color online) Temperature vs target length at $t = 7850$ ns, when 144 bunches have been delivered; (a) at $r = 0.0$ (axis), (b) at $r = 1$ mm, and (c) at $r = 2$ mm.

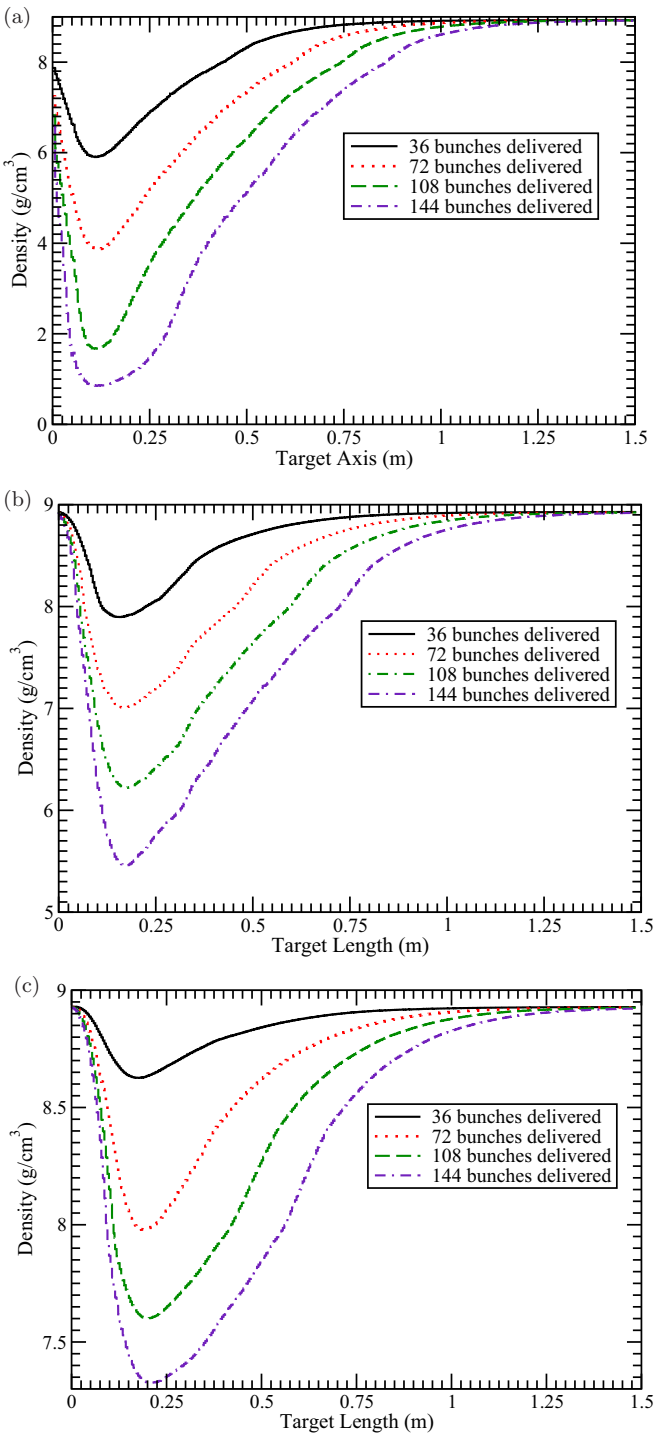

FIG. 7. (Color online) Density vs target length at $t = 7850$ ns, when 144 bunches have been delivered; (a) at $r = 0.0$ (axis), (b) at $r = 1$ mm, and (c) at $r = 2$ mm.

and corresponds to the conditions in Experiment 3. It is seen that different phase states of copper exist in different parts of the target in the beam heated region. These include melting phase, compressed as well as expanded hot liquid states, two-phase liquid-gas state, and gaseous phase. Figure 9 presents a photograph of the gap between cylinder 4 and cylinder 5 of Target 3 in Experiment 3 (after the delivery of 144 bunches). It is seen that holes are generated at the faces of the cylinders and the ejected material (melted or evaporated copper), is deposited at the surface, which has been solidified. This confirms the simulations that predict the generation of HED states in the target in the HiRadMat beam-matter interaction experiments.

C. Comparison between experimental measurements and simulation results

In this subsection we provide a brief comparison between the experimental measurements and the simulation results.

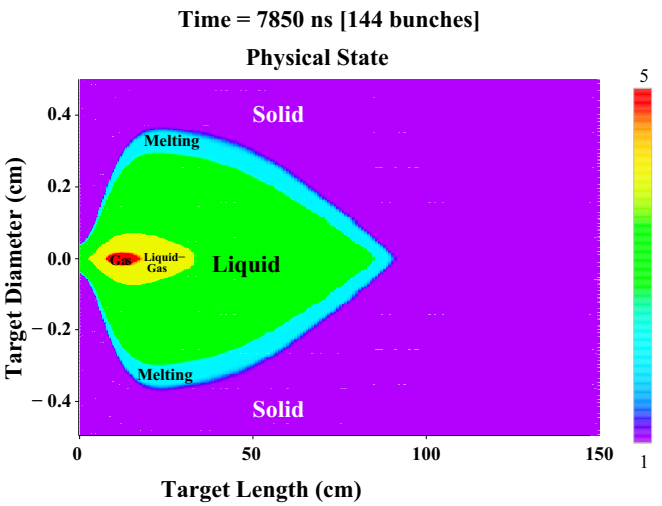

FIG. 8. (Color online) Target physical state at $t = 7850$ ns, when 144 bunches have been delivered.

Further details about the experiments can be found in [47,48]. The beam is incident vertically on the face of the first cylinder coaxially and the projectile particles, together with their hadronic shower, penetrate deep into the target. A visual inspection of the Al target cover that was placed at the top of the targets revealed some interesting features of the experiment. A photograph of the inner surface of the cover is presented in Fig. 10 that shows traces of copper deposited above the gaps between the cylinders. It is seen that in the case of the experiment using 144 bunches and beam focal spot $\sigma = 2.0$ mm (bottom picture), the splash of molten copper occurs up to the gap between the fifth and the sixth cylinder. That means that the material was molten or evaporated over a length of 55 ± 5 cm. In the second experiment with 108 bunches and beam focal spot, $\sigma = 0.2$ mm (middle picture), the molten or evaporation zone goes up to the eighth cylinder that means a damage length of 75 ± 5 cm. In the experiment with 144 bunches and beam focal spot, $\sigma = 0.2$ mm (top picture), the molten or evaporation zone is extended to the ninth cylinder, that means a damage length of 85 ± 5 cm.

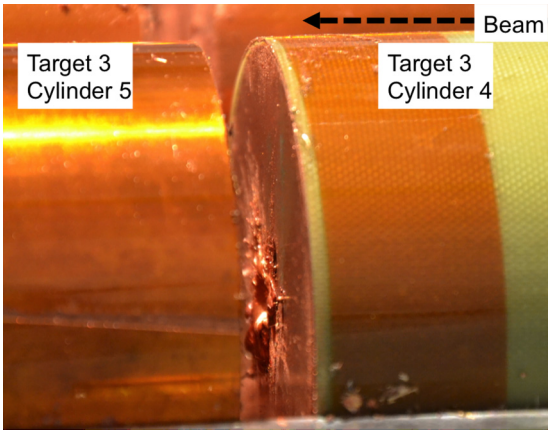

FIG. 9. (Color online) Picture showing gap between cylinders 4 and 5 of Target 3 (Experiment 3), holes generated on the faces of the cylinders, and the ejection of molten or evaporated copper which has been solidified at the surface, is clearly visible.

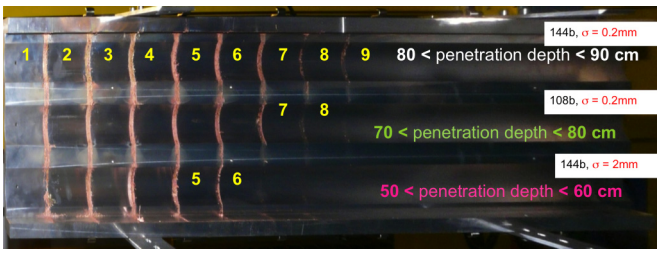

FIG. 10. (Color online) Top cover of the experimental setup after the irradiation. Traces of projected copper between the 10-cm-long cylinders of the targets indicate the length of the melting or evaporation zone. For Target 1 (bottom) the molten or evaporation zone ends in the sixth cylinder, i.e., the copper was molten over a length of 55 ± 5 cm. For Target 2 (mid) the molten zone goes up to cylinder 8, i.e., 75 ± 5 cm. For Target 3 (top) the molten zone goes up to cylinder 9, i.e., 85 ± 5 cm.

In Fig. 11(a) are plotted the density ρ and the temperature T along the axis at $t = 5800$ ns obtained in the simulations, when 108 bunches have been delivered for Experiment 2 (using $\sigma = 0.2$ mm). It is seen that the flat part of the temperature curve

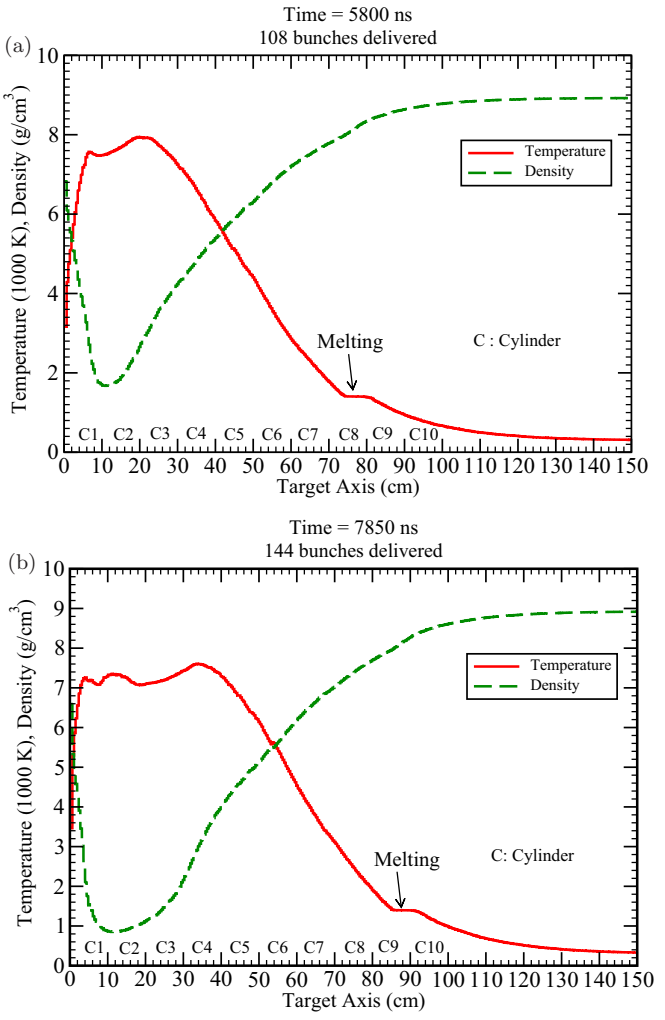

FIG. 11. (Color online) (a) ρ and T vs target axis at $t = 5800$ ns (108 bunches); (b) ρ and T vs target axis at $t = 7850$ ns (144 bunches).

that represents melting region lies within $L = 75$ and 80 cm that is equivalent to the RHS half of the eighth cylinder. The temperature curve also shows that the material along the axis up to 75 cm is liquefied or even evaporated, depending on the value of the temperature. The liquefied material escapes from the left face of cylinder number 8 and collides with the melted or gaseous material ejected from the right face of cylinder number 7. As a result of this collision, the material is splashed vertically and is deposited at the inner surface of the target cover above the gap between cylinder numbers 7 and 8. The simulations are therefore in full agreement with the experimental observations.

It is also interesting to note that there is a very weak trace of matter in the bottom half of the middle strip (Target 2 in Fig. 10) above the gap between cylinders 8 and 9. This in fact is a tiny amount of matter that originates from the gap between cylinders 8 and 9 of Target 3 and is deposited at this place. Otherwise, the trace would be much thicker and would be along the full length of the gap. Moreover, visual inspection of the target has shown that the opposite faces of cylinders 8 and 9 in Target 2 are not damaged at all.

Figure 11(b) shows the same variables as Fig. 11(a), but at $t = 7850$ ns when 144 bunches have been delivered. The melting region now lies between $L = 85$ and 90 cm, which is the RHS half of cylinder 9 while the left half part ($L =$ 80–85 cm) has been liquefied. The simulations thus predict material deposition at the inner surface of the target cover above the region between cylinders 8 and 9, which is in full agreement with the experimental measurements. These experiments therefore confirm the existence of the hydrodynamic tunneling in case of the SPS beam in accordance with the theoretical predictions. The results thus give confidence in the numerical simulations for more powerful LHC reported in [45].

It is also worth mentioning that for HED physics studies, direct measurement of the physical parameters including density, temperature and pressure, and comparison with the simulations will be more useful, but this requires the availability of the necessary diagnostic tools, which at present is not possible. However, this is intended for the future work.

VI. CONCLUSIONS

Unique experiments have been done at the CERN HiRadMat facility to study interaction of 440-GeV ultrarelativistic proton beam delivered by the SPS, with extended solid copper cylindrical targets. These experiments have provided the first experimental proof of the existence of the hydrodynamic tunneling of the protons in the target. The experimental measurements, together with a comparison with numerical simulations, have been reported in [47,48], that show excellent agreement between the two. In the present paper, the details about the numerical simulations of these experiments are provided that give information about the physical state of the target material, during and after the irradiation. Two experimental cases have been considered in the simulation studies. These simulations show that due to the strong heating caused by the high level of energy deposited by the beam, the material in the beam heated region undergoes different phase transitions, thereby generating samples with extreme states of HED copper. It is thus concluded that the HiRadMat facility can be used to perform dedicated experiments to research the field of HED physics. This work is intended for the future.

ACKNOWLEDGMENTS

The authors would like to thank the BMBF and the EuCARD2 for providing the financial support for doing this work.

[1] The LHC Design Report, technical report (CERN, Geneva, 2004).
[2] W. F. Henning, Nucl. Inst. Meth. B **214**, 211 (2004).
[3] J. Steinheimer, J. Phys. G **37**, 094026 (2010).
[4] FAIR baseline technical report (GSI, Darmstadt, Germany, 2006).
[5] L. Maunoury, P. Delahaye, J. Angot, B. Dubois, M. Dupuis, R. Frigot, J. Grnyer, P. Jardin, C. Leboucher, and T. Lamy, Rev. Sci. Instrum. **85**, 02A504 (2014).
[6] R. Schmidt, R. Assmann, E. Carlier, B. Dehning, R. Denz, B. Goddard, E. B. Holzer, V. Kain, B. Puccio, and B. Todd *et al.*, New J. Phys. **8**, 290 (2006).
[7] H. K. Mao and R. J. Hemley, Rev. Mod. Phys. **66**, 671 (1994).
[8] C. Narayan, H. Luo, and A. L. Ruoff, Nature (London) **393**, 46 (1998).
[9] M. van Thiel, "Compendium of shock wave data," technical report (University of California Radiation Laboratory, Berkeley, 1977).
[10] W. J. Nellis, A. C. Mitchell, P. C. McCandless, D. J. Erskine, and S. T. Weir, Phys. Rev. Lett. **68**, 2937 (1992).
[11] M. D. Knudson, D. L. Hanson, J. E. Bailey, C. A. Hall, J. R. Asay, and W. W. Anderson, Phys. Rev. Lett. **87**, 225501 (2001).
[12] R. Cauble, D. W. Phillion, T. J. Hoover, N. C. Holmes, J. D. Kilkenny, and R. W. Lee, Phys. Rev. Lett. **70**, 2102 (1993).
[13] M. Koenig, B. Faral, J. M. Boudenne, D. Batani, A. Benuzzi, S. Bossi, C. Remond, J. P. Perrnie, M. Temporal, and S. Atzeni, Phys. Rev. Lett. **74**, 2260 (1995).
[14] A. S. Vladimirov, N. P. Voloshin, V. N. Nogin, A. P. Petrovtsev, and V. A. Simonenko, JETP Lett. **39**, 85 (1984).
[15] N. A. Tahir, C. Deutsch, V. E. Fortov, V. Gryaznov, D. H. H. Hoffmann, M. Kulish, I. V. Lomonosov, V. Mintsev, P. Ni, D. Nikolaev, A. R. Piriz, N. Shilkin, P. Spiller, A. Shutov, M. Temporal, V. Ternovoi, S. Udrea, and D. Varentsov, Phys. Rev. Lett. **95**, 035001 (2005).
[16] N. A. Tahir, V. Kain, R. Schmidt, A. Shutov, I. V. Lomonosov, V. Gryaznov, A. R. Piriz, M. Temporal, D. H. H. Hoffmann, and V. E. Fortov, Phys. Rev. Lett. **94**, 135004 (2005).
[17] J. J. Barnard, J. Armijo, R. M. More, A. Friedman, I. Kaganovich, B. G. Logan, M. M. Marinak, G. E. Penn, A. B. Sefkow, and P. Santhanam *et al.*, Nucl. Instr. Meth. A **577**, 275 (2007).
[18] N. A. Tahir, D. H. H. Hoffmann, J. A. Maruhn, K.-J. Lutz, and R. Bock, Phys. Plasmas **5**, 4426 (1998).
[19] N. A. Tahir, D. H. H. Hoffmann, J. A. Maruhn, P. Spiller, and R. Bock, Phys. Rev. E **60**, 4715 (1999).

[20] N. A. Tahir, D. H. H. Hoffmann, A. Kozyreva, A. Shutov, J. A. Maruhn, U. Neuner, A. Tauschwitz, P. Spiller, and R. Bock, Phys. Rev. E **61**, 1975 (2000).
[21] N. A. Tahir, D. H. H. Hoffmann, A. Kozyreva, A. Shutov, J. A. Maruhn, U. Neuner, A. Tauschwitz, P. Spiller, and R. Bock, Phys. Rev. E **62**, 1224 (2000).
[22] N. A. Tahir, D. H. H. Hoffmann, A. Kozyreva, A. Tauschwitz, A. Shutov, J. A. Maruhn, P. Spiller, U. Neuner, J. Jacoby, M. Roth, R. Bock, H. Juranik, and R. Redmer, Phys. Rev. E **63**, 016402 (2001).
[23] N. A. Tahir, A. Kozyreva, P. Spiller, D. H. H. Hoffmann, and A. Shutov, Phys. Rev. E **63**, 036407 (2001).
[24] N. A. Tahir, A. Shutov, D. Varentsov, P. Spiller, S. Udrea, D. H. H. Hoffmann, I. Lomonosov, J. Wieser, M. Kirk, R. Piriz, V. E. Fortov, and R. Bock, Phys. Rev. ST Accel. Beams **6**, 020101 (2003).
[25] N. A. Tahir, P. Spiller, A. Shutov, I. V. Lomonosov, V. Gryaznov, A. R. Piriz, G. Wouchuk, C. Deutsch, V. E. Fortov, D. H. H. Hoffmann, and R. Schmidt, Nucl. Inst. Meth. A **577**, 238 (2007).
[26] N. A. Tahir, Th. Stöhlker, A. Shutov, I. V. Lomonosov, V. E. Fortov, M. French, N. Nettelmann, R. Redmer, A. R. Piriz, and C. Deutsch *et al.*, New J. Phys. **12**, 073022 (2010).
[27] N. A. Tahir, A. Shutov, A. P. Zharkov, A. R. Piriz, and Th. Stöhlker, Phys. Plasmas **18**, 032704 (2011).
[28] R. O. Bangerter, J. W. K. Mark, and A. R. Thiessen, Phys. Lett. A **88**, 225 (1982).
[29] N. A. Tahir and K. A. Long, Nucl. Fusion **23**, 887 (1983).
[30] N. A. Tahir and K. A. Long, Laser Part. Beams **2**, 371 (1984).
[31] N. A. Tahir and K. A. Long, Z. Phys. A **325**, 99 (1986).
[32] C. Deutsch, Ann. Phys. Fr. **11**, 1 (1986).
[33] B. G. Logan, L. J. Perkins, and J. J. Barnard, Phys. Plasmas **15**, 072701 (2008).
[34] A. R. Piriz, Phys. Fluids **31**, 658 (1988).
[35] A. R. Piriz and M. M. Sanchez, Phys. Plasmas **5**, 2721 (1998).
[36] N. A. Tahir, H. Weick, H. Iwase, H. Geissel, D. H. H. Hoffmann, B. Kindler, B. Lommel, T. Radon, G. Münzenberger, A. Shutov, K. Sümmerer, and M. Winkler, J. Phys. D **38**, 1828 (2005).
[37] N. A. Tahir, V. V. Kim, A. V. Matveichev, A. V. Ostrik, A. V. Shutov, I. V. Lomonosov, A. R. Piriz, J. J. Lopez Cela, and D. H. H. Hoffmann, Laser Part. Beams **26**, 273 (2008).
[38] N. A. Tahir, H. Weick, A. Shutov, V. Kim, A. Matveichev, A. Ostrik, V. Sultanov, I. V. Lomonosov, A. R. Piriz, J. J. Lopez Cela, and D. H. H. Hoffmann, Laser Part. Beams **26**, 411 (2008).
[39] N. A. Tahir, A. Matveichev, V. Kim, A. Ostrik, A. Shutov, V. Sultanov, I. V. Lomonosov, A. R. Piriz, and D. H. H. Hoffmann, Laser Part. Beams **27**, 9 (2009).
[40] H. Geissel, H. Weick, M. Winkler, G. Münzenberg, V. Chichkine, M. Yavor, T. Aumann, K. A. Behr, M. Bohmer, A. Brunle, K. Burhard, J. Benlliure, D. Gill-Cortina, L. Chulkov, A. Dael, J. E. Ducret, H. Emling, B. Franczak, J. Friese, B. Castineau, R. Gernhauser, M. Hellstrom, B. Johnson, J. Kojouharova, R. Kullesa, B. Kindler, N. Kurz, B. Lommel, W. Mittig, G. Moritz, C. Mühle, J. A. Nolen, G. Nyman, P. Roussel-Chomaz, C. Scheidenberger, K. H. Schmidt, G. Schrieder, B. M. Sherrill, H. Simon, K. Sümmerer, N. A. Tahir, V. Vysotsky, H. Wolnik, and A. F. Zeller, Nucl. Inst. Meth. B **204**, 71 (2003).
[41] N. A. Tahir, V. Kim, E. Lamour, I. V. Lomonosov, A. R. Piriz, J. P. Rozet, Th. Stöhlker, V. Sultanov, and D. Vernhet, Nuclear Inst. Meth. B **276**, 66 (2012).
[42] N. A. Tahir, V. Kim, E. Lamour, I. V. Lomonosov, A. R. Piriz, J. P. Rozet, Th. Stöhlker, V. Sultanov, and D. Vernhet, Nuclear Inst. Meth. B **290**, 43 (2012).
[43] N. A. Tahir, V. Kim, B. Schlitt, W. Barth, L. Groening, I. V. Lomonosov, A. R. Piriz, T. Stöhlker, and H. Vormann, Phys. Rev. ST Accel. Beams **17**, 041003 (2014).
[44] N. A. Tahir, R. Schmidt, A. Shutov, I. V. Lomonosov, A. R. Piriz, D. H. H. Hoffmann, C. Deutsch, and V. E. Fortov, Phys. Rev. E **79**, 046410 (2009).
[45] N. A. Tahir, J. Blanco Sancho, A. Shutov, R. Schmidt, and A. R. Piriz, Phys. Rev. ST Accel. Beams **18**, 032704 (2012).
[46] N. A. Tahir, B. Goddard, V. Kain, R. Schmidt, A. Shutov, I. V. Lomonosov, A. R. Piriz, M. Temporal, D. H. H. Hoffmann, and V. E. Fortov, J. Appl. Phys. **97**, 083532 (2005).
[47] R. Schmidt, J. Blanco Sancho, F. Burkart, D. Grenier, D. Wollmann, N. A. Tahir, A. Shutov, and A. R. Piriz, Phys. Plasmas **21**, 080701 (2014).
[48] R. Schmidt, J. Sancho Blanco, F. Burkart, D. Grenier, D. Wollmann, and N. A. Tahir, in *Proceedings of IPAC13* (JACoW, Shanghai, China, 2013).
[49] A. Fasso, A. Ferrari, J. Ranft, and P. R. Sala, technical report (CERN, Geneva, 2005).
[50] A. Fasso, A. Ferrari, S. Roesler, R. P. Sala, G. Battistoni, F. Cerutti, E. Gadioli, M. V. Garzelli, F. Ballarini, A. Ottolenghi, A. Empl, and J. Ranft, in *Conference on Computing in High Energy and Nuclear Physics* (UCSD, La Jolla, 2003).
[51] V. E. Fortov, B. Goel, C. D. Munz, A. L. Ni, A. Shutov, and O. V. Vorobiev, Nucl. Sci. Eng. **123**, 169 (1996).
[52] I. V. Lomonosov, Laser Part. Beams **25**, 567 (2007).
[53] I. V. Lomonosov and N. A. Tahir, Appl. Phys. Lett. **92**, 101905 (2008).